JOURNAL OF GEOPHYSICAL RESEARCH, VOL. 115, B02202, doi:10.1029/2009JB006302, 2010

Partitioning of oxygen between the Earth's mantle and core

Daniel J. Frost,[1] Yuki Asahara,[2,3] David C. Rubie,[1] Nobuyoshi Miyajima,[1] Leonid S. Dubrovinsky,[1] Christian Holzapfel,[4,5] Eiji Ohtani,[6] Masaaki Miyahara,[6] and Takeshi Sakai[6]

Received 12 January 2009; revised 27 June 2009; accepted 30 September 2009; published 10 February 2010.

[1] Experiments to investigate the partitioning of oxygen between liquid iron and (Mg,Fe)O magnesiowüstite were conducted at 30–70 GPa and 2800–3500 K using a laser-heated diamond anvil cell. A thin foil was prepared from the reacted regions in the recovered samples using a focused ion beam. The compositions of coexisting quenched iron and magnesiowüstite were measured using a transmission electron microscope equipped with energy dispersive X-ray spectroscopy and electron energy-loss spectroscopy. In order to understand and model the results, additional experiments were performed to determine the activity of oxygen, or rather FeO, in liquid Fe metal. Multianvil experiments to measure the oxygen contents of coexisting immiscible metallic and ionic liquids in the Fe-FeO system were performed up to 25 GPa. The results were used to extract excess mixing properties for Fe-FeO liquids at high pressure and temperature. These properties were used to derive a model that describes oxygen partitioning in the Fe-Mg-O system that is independent of the actual experimental partitioning data. The model indicates that the oxygen content of liquid Fe becomes a strong nonlinear function of the FeO content of magnesiowüstite at pressures greater than 25 GPa. This prediction is in excellent agreement with the experimental partitioning data, which is faithfully reproduced in most instances. The new results confirm that the Earth's core is undersaturated in oxygen with respect to the FeO content of the bulk mantle, which will result either in FeO being depleted from the very base of the mantle or lead to the development of an FeO-enriched outer layer of the core. These possibilities are not mutually exclusive.

Citation: Frost, D. J., Y. Asahara, D. C. Rubie, N. Miyajima, L. S. Dubrovinsky, C. Holzapfel, E. Ohtani, M. Miyahara, and T. Sakai (2010), Partitioning of oxygen between the Earth's mantle and core, *J. Geophys. Res.*, *115*, B02202, doi:10.1029/2009JB006302.

1. Introduction

[2] Oxygen is potentially an important light element in the Earth's outer core [e.g., *Ringwood*, 1977], and its partitioning during accretion and core-mantle fractionation may have controlled the FeO content of the mantle [*Rubie et al.*, 2004]. There are two principle arguments for the presence of at least some oxygen in the core: (1) As oxygen partitions more strongly into liquid over solid metallic Fe, its presence can explain, to some extent, the density difference between the inner and outer core [*Alfè et al.*, 2002a]. (2) Dynamic simulations of the Moon-forming impact indicate that most of the mass of the Moon came from a Mars-sized impactor termed Theia [*Canup and Asphaug*, 2001], which oxygen isotopes indicate may have formed from similar material as the Earth [*Wiechert et al.*, 2001]. The Moon might, therefore, be viewed as a preserved embryo of the Earth in an earlier stage of its development. If this is the case, the FeO-rich nature of the Moon's mantle, revealed through lunar basalts, compared with the Earth's could be explained if oxygen was extracted to the core at some later stage of the Earth's development [*Halliday*, 2007].

[3] While many efforts have been made to determine the identity of the light elements in the core from the geophysical considerations provided by seismology [e.g., *Birch*, 1952; *Alfè et al.*, 2002a], additional constraints also come from geochemical arguments for the partitioning of light elements between the mantle and core during accretion and core formation. To constrain the oxygen content of the core through such geochemical considerations requires information on the oxygen content of liquid iron in equilibrium with silicates at the relevant pressures, temperatures, and oxygen fugacities. The pressures at which the metal and silicate equilibrated during core formation may have ranged up to those of the present-day core-mantle boundary (136 GPa), while the temperatures may have significantly exceeded the

[1] Bayerisches Geoinstitut, Universität Bayreuth, Bayreuth, Germany.
[2] Japan Synchrotron Radiation Research Institute, Hyogo, Japan.
[3] High Pressure Material Physics Group, Department of Earth and Space Science, Graduate School of Science, Osaka University Toyonaka, Japan.
[4] Institut für Werkstoffwissenschaft, Universität Saarlandes, Saarbrücken, Germany.
[5] Now at Schleifring und Apparatebau GmbH, Fürstenfeldbruck, Germany.
[6] Institute of Mineralogy, Petrology and Economic Geology, Tohoku University, Sendai, Japan.

0148-0227/10/2009JB006302$09.00

current values in this region, i.e., >4000 K [*Rubie et al.*, 2007]. Oxygen partitioning between liquid iron and either magnesiowüstite or magnesium silicate perovskite has been investigated through high-pressure experiments by several workers over a wide pressure and temperature range, 2–139 GPa, 2273–3150 K [e.g., *Ohtani and Ringwood*, 1984; *Rubie et al.*, 2004; *Takafuji et al.*, 2005, *Sakai et al.*, 2006; *Asahara et al.*, 2007]. Many studies have used magnesiowüstite as a proxy for silicate liquids as liquids are hard to encapsulate during experiments at very high temperatures. *Asahara et al.* [2007] proposed a simple semiempirical model based on the available oxygen partitioning studies but because this also employed data on the oxygen content of liquid iron coexisting with either the perovskite or post-perovskite phase, some uncertainty remained in its applicability because the oxygen fugacity is not buffered in such experiments. Recently, *Ozawa et al.* [2008] reported diamond anvil cell measurements of oxygen partitioning between magnesiowüstite and liquid iron up to 134 GPa. The model of *Asahara et al.* [2007] is in poor agreement with these data although it shows a similar qualitative trend.

[4] In this study, we have employed the laser-heated diamond anvil cell (LHDAC) to investigate oxygen partitioning between magnesiowüstite and liquid iron up to 70 GPa and 3500 K. A focused ion beam (FIB) was used to prepare thin foils from run products for analysis using transmission electron microscopy (TEM). As our results are only in qualitative agreement with the model of *Asahara et al.* [2007], we were led to consider a more complex thermodynamic analysis of the data. Oxygen partitioning is normally described using a distribution coefficient K_D defined as

$$K_D = \frac{X_{\mathrm{Fe}}^{\mathrm{met}} X_{\mathrm{O}}^{\mathrm{met}}}{X_{\mathrm{FeO}}^{mw}}, \quad (1)$$

where X_{FeO}^{mw}, $X_{\mathrm{Fe}}^{\mathrm{met}}$, and $X_{\mathrm{O}}^{\mathrm{met}}$ are the mole fractions of FeO in magnesiowüstite and Fe and O in liquid metal, respectively. The advantage of using K_D is that it has been shown, in experiments up to 25 GPa [*Asahara et al.*, 2007], to be nominally independent of oxygen fugacity (fo_2), which is a major simplifying assumption employed in models describing such data [*Asahara et al.*, 2007; *Ozawa et al.*, 2008]. This independence arises because the activity coefficient term that describes the nonideality of oxygen mixing in liquid iron metal remains approximately constant over the solute concentration range of interest, i.e., Henry's law is followed. Mixing in both oxide and metallic phases is nonideal, however, as is demonstrated in the case of liquid iron by the presence of a large region of immiscibility between liquid Fe-rich metal and FeO-rich ionic liquid at ambient pressure. Several studies have presented evidence that this compositional gap closes with increasing pressure [*Ohtani et al.*, 1984; *Kato and Ringwood*, 1989; *Takahashi et al.*, 2004; *Tsuno et al.*, 2007], which must be accompanied by relatively large changes in the activity-composition relations in the Fe-O system. An independent assessment of the effect of pressure on the compositional dependence of K_D could be made using data on the phase relations of the immiscible liquids in the Fe-O system at high pressures and temperatures. We have, therefore, performed additional experiments in the Fe-O system to determine the liquid-phase relations to pressures of 25 GPa in a multianvil apparatus. These data are used to extract activity-composition relations for Fe-O mixing, which are then combined with additional literature data to produce a model to describe oxygen partitioning between magnesiowüstite and liquid iron metal that is completely independent of the experimental partitioning data. This model reproduces the LHDAC data very well and has a suitable theoretical basis to be extrapolated over wider ranges of conditions than empirical models.

2. Experimental and Analytical Procedures

2.1. Laser-Heated Diamond Anvil Cell Experiments

[5] We used pure iron foil with a thickness of 5 μm and sintered magnesiowüstite pellets with three different compositions, i.e., $Mg_{0.98}Fe_{0.02}O$, $Mg_{0.95}Fe_{0.05}O$, and $Mg_{0.93}Fe_{0.07}O$, as starting materials. Magnesiowüstite powders, with the required compositions, were synthesized from mixtures of Fe_2O_3 and MgO in a gas-mixing furnace at 1200°C with the oxygen fugacity set at the iron-wüstite buffer. The resulting powders were then sintered using a multianvil apparatus at 24 GPa and 2000°C. High pressure and the use of graphite as the sample container ensured a low Fe^{3+} content in the samples. Pellets with a thickness of approximately 20 μm and polished on both sides were prepared from the recovered samples.

[6] High-pressure, high-temperature experiments were conducted using diamond anvil cells with laser-heating systems at both the Bayerisches Geoinstitut (BGI) and Tohoku University. Experimental conditions and results are summarized in Table 1.

[7] The sample assembly used for the laser-heating experiments is shown in Figure 1. Fe foil sandwiched between two magnesiowüstite pellets was loaded in a gasket hole with a diameter of 150 μm. NaCl powder was used as the pressure medium and as a thermal insulator. A small ruby sphere was placed on the surface of one diamond for pressure calibration. We loaded the cell in an argon atmosphere to avoid contamination by air. We used a YLF laser at BGI and a Nd:YAG laser at Tohoku University to heat the samples in the diamond anvil cells. Single-sided laser heating was employed at BGI, and double-sided laser heating was used at Tohoku University. Temperatures were measured by spectroradiometry. Pressures were determined by the ruby fluorescence method [*Mao et al.*, 1978] at room temperature before and after heating.

[8] Each recovered sample, still contained in the gasket, was mounted in epoxy and a section through the center of the sample was polished for scanning electron microscopic observations. The region of each sample that had been laser heated was removed from the polished section as a small film (height 5 μm, width 15 μm, thickness 80–200 nm) using FIB-milling systems at the Universities of Saarland and Tohoku (see Figure 2). Transmission electron microscopy of the foils was performed using a Philips CM20 FEG TEM operating at 200 kV at BGI. It was possible to perform chemical mapping using scanning transmission microscopy (STEM) on the thin foil obtained by FIB but the foil was too thick (>100 nm) for electron energy-loss spectroscopy (EELS) analysis for obtaining oxygen concentrations in quenched liquid Fe. Therefore, after chemical mapping,

Table 1. Conditions and Results of Diamond Anvil Cell Experiments

	Run			
	M95I30[a]	M93I30[a]	M98I65[b]	M95I70[a]
Starting composition, X_{FeO}^{mw}	0.05	0.07	0.02	0.05
Pressure (GPa)				
Before heating	30	33	70	72
After heating	26	29	62	68
Mean[c]	28	31	66	70
Temperature (K)	2800	2800	3100	3500
Error	200	200	100	300
Compositions of run products				
n[d]	7	15	7	3
X_{FeO}^{mw}	0.076	0.059	0.035	0.191
Error	0.008	0.012	0.018	0.013
n	6	11	3	6
X_O^{met}	0.063	0.045	0.047	0.241
Error	0.022	0.010	0.007	0.068
Ln K_D	−0.25	−0.33	0.25	−0.04
Error	0.45	0.42	0.69	0.26

[a]Experiments conducted at Bayerisches Geoinstitut.
[b]Experiments conducted at Tohoku University.
[c]Mean pressure was treated as the experimental pressure.
[d]Number of measurements.

we thinned the foil again using conventional argon milling to a thickness of 80–40 nm. Quantitative chemical analysis with energy-dispersive X-ray spectroscopy on magnesiowüstite was carried out in the TEM mode. The k factors were calibrated using the parameter-less correction method of *van Cappellen* [1990]. The absorption correction was performed following the procedure of *van Cappellen and Doukhan* [1994]. Elemental mapping for Fe, Mg, O, and C was performed in the STEM mode. Concentrations of oxygen in quenched liquid iron were obtained by EELS. The partial scattering cross-section ratio between oxygen and iron was determined experimentally by using a $Fe_{0.94}O$ standard. All EELS spectra for quantitative oxygen analysis were collected under the following operating conditions: 8.0 mrad convergent angle (2α), 4.3 mrad spectrometer collection angle (2β), and 1–3 s integration time per readout. Spectral processing included subtraction of the dark current, alignment and summation of offset spectra to reduce channel-to-channel

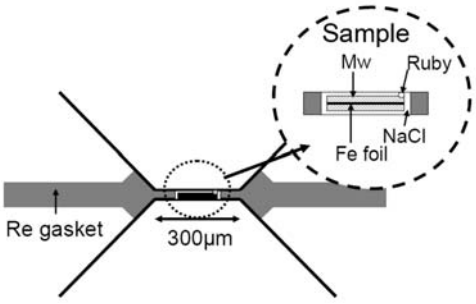

Figure 1. Schematic illustration of the laser-heated DAC sample assembly.

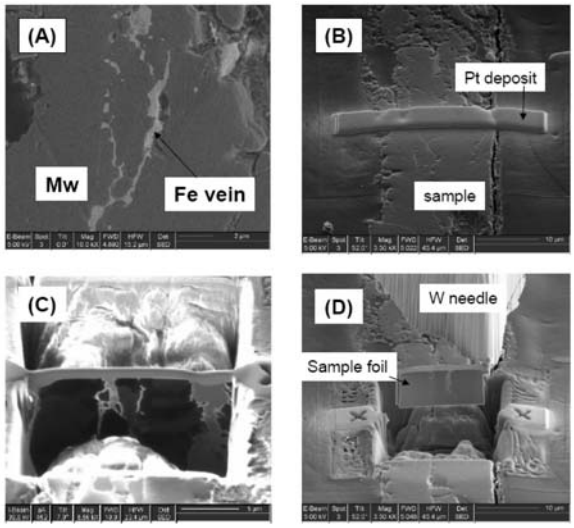

Figure 2. Thin foil preparation procedure using the FIB-milling system. (a) Scanning electron image of a polished section of the recovered sample from the experiment at 31 GPa and 2800 K (run: M93I30). The thickness of the recovered samples was 15–20 μm, and quenched liquid Fe is distributed in the sample as thin veins with a thickness of less than 1 μm and/or as small inclusions. When extracting thin foils for TEM analysis using FIB, we chose regions that contained magnesiowüstite coexisting with metallic veins that were free of fractures. The long side of the image (LSI) is 14 μm. (b) Overview of the platinum coating that is deposited on the selected region before thinning with a Ga^+ beam. LSI = 43 μm. (c) Overview of the sample foil after thinning. A metallic vein in the magnesiowüstite can be observed. LSI = 23 μm. (d) Removing the foil from the host sample using a tungsten needle. LSI = 43 μm.

gain variations, and background subtractions of the form AE^{-g} [*Egerton*, 1996]. Technical details of the FIB milling and EELS method are described by *Miyajima et al.* [2010].

2.2. Multianvil Fe-O Liquid Phase Relations

[9] Starting materials were mixtures of Fe and Fe_2O_3 ground in the correct proportions to produce two compositions containing 5 and 9 wt% oxygen. Fe_2O_3 was prepared by firing the reagent-grade oxide at 1000°C for 3 h. Both samples were loaded into Al_2O_3 capsules containing two sample chambers. The capsules were made from two-hole thermocouple ceramic cut into 1 mm long sections and closed at both ends with 0.3 mm thick Al_2O_3 disks. The Al_2O_3 capsules were run in a Kawai-type multianvil apparatus at the BGI. To pressures of 20 GPa, a 10 mm edge length Cr_2O_3-doped MgO octahedral pressure assembly was employed with 5 mm edge length tungsten carbide anvil truncations. At 24.5 GPa, a similar octahedron was employed with 4 mm edge length cube truncations. A $LaCrO_3$ resistance heater was used with a $W_{97}Re_3$-$W_{75}Re_{25}$ thermocouple. Samples were heated for a few minutes and then quenched rapidly by turning off the power to the heater. Recovered samples were mounted in epoxy resin and then sectioned and polished for analysis with a scanning electron

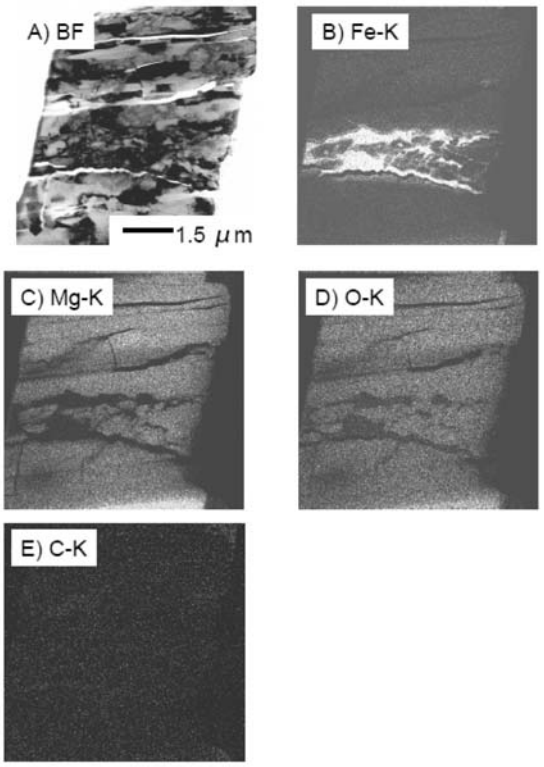

Figure 3. Elemental mapping images of a thin foil prepared by the FIB milling technique from the sample that was reacted at 70 GPa and 3500 K (run: M95I70). (a) Bright field transmission electron micrograph of the mapped area. (b) Distribution of Fe; (c) distribution of Mg; (d) distribution of O; (e) distribution of C.

microscope and an electron microprobe. Chemical analyses were obtained using a JEOL JXA-8200 electron microprobe at 20 kV and 50 nA with counting times of 20 s. Fe and O standards were Fe metal and periclase, respectively. The liquid samples fully crystallize on quenching into heterogeneous mats of quench crystals that were analyzed using a 10 μm defocused beam.

3. Results

3.1. Laser-Heated Diamond Anvil Cell

3.1.1. Attainment of Equilibrium

[10] Although we used two different laser-heating methods, i.e., double-sided heating and single-sided heating, there are no distinct differences between the features of the reacted regions obtained by these two techniques. Fe was dispersed as thin veins (<1 μm wide) during heating and reacted with the surrounding magnesiowüstite (see Figure 2a). Across such thin veins, the temperature gradient must have been negligible. The duration of laser heating was about 5 min in all experiments. This is sufficient for attaining equilibrium between coexisting metallic liquid and magnesiowüstite based on a time study performed using multianvil experiments [*Gessmann and Rubie*, 1998]. In addition, we obtained consistent results at similar $P - T$ conditions using different starting compositions (runs: M95I30 and M93I30). This also indicates that equilibrium was achieved during the high-temperature experiments.

3.1.2. Composition of Magnesiowüstite Adjacent to Iron

[11] Initially, we performed chemical mapping for Fe, Mg, O, and C using STEM and checked the element distribution over the entire sample foil. Figure 3 shows representative chemical mapping images. In most cases, magnesiowüstite immediately adjacent to iron was enriched in FeO, even though the starting material consisted of magnesiowüstite and pure iron. Some oxidation of the sample evidently occurred at high pressure and temperature. However, the presence of excess oxygen should not affect the attainment of chemical equilibrium between liquid iron and magnesiowüstite. There are several possibilities for the origin of excess oxygen, such as oxidation from trace H_2O

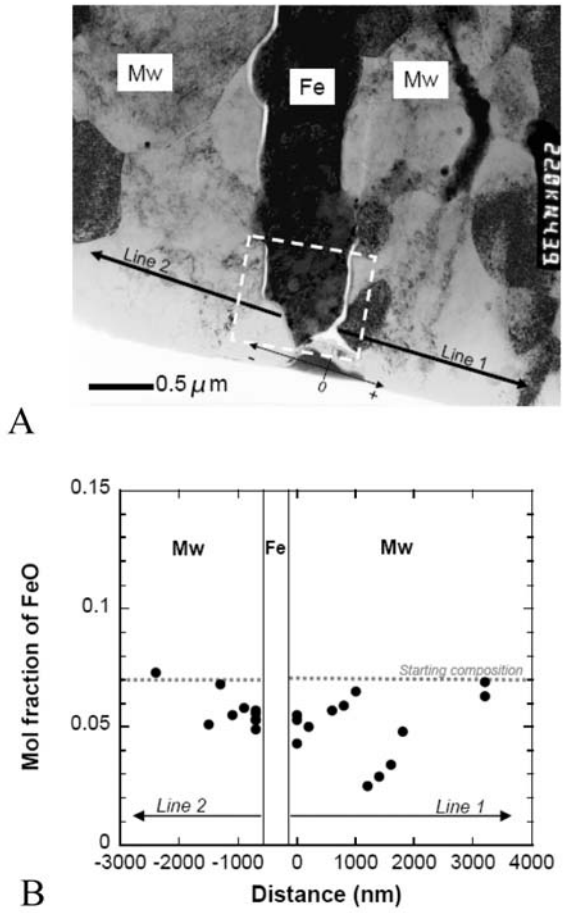

Figure 4. (a) Bright field transmission electron micrograph of the thin foil obtained from the sample reacted at 31 GPa and 2800 K (run: M93I30). Compositional profiles in magnesiowüstite (Mw) were obtained along lines 1 and 2. The dashed square indicates the region in which EELS analysis was performed. (b) Compositional profile of FeO in magnesiowüstite along lines 1 and 2 as indicated in Figure 4a. The concentration of FeO is reduced relative to the starting composition ($Mg_{0.93}Fe_{0.07}O$) near the interfaces with iron. Along line 1 at a distance of 1000–2000 nm from iron, low concentrations of FeO are also observed that might indicate the proximity of another iron vein outside the plane of the section though the spatial variation of oxygen is relatively large.

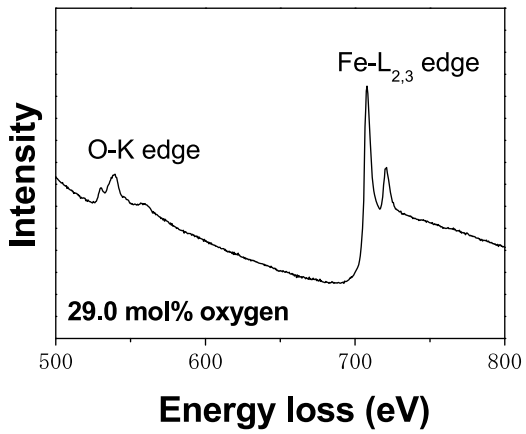

Figure 5. Representative EELS spectrum of quenched iron in the thin foil from the sample reacted at 70 GPa and 3500 K (run: M95I70). Based on this spectrum, 29 mol% of oxygen was detected.

absorbed into the starting powders or oxidation of the iron foil. In the absence of such oxidation, FeO was removed from the magnesiowüstite to become dissolved in the liquid iron. In this case, the change of FeO distribution in magnesiowüstite adjacent to an Fe vein was difficult to observe with chemical mapping because the strong intensity of Fe from the metallic vein masked the weak contrast variation in magnesiowüstite. However, line profiles obtained by spot analyses indicate that the FeO content of the magnesiowüstite was reduced by reaction with liquid Fe (see Figure 4). The thickness of such reaction rims in the magnesiowüstite was generally less than 1 μm in all samples. We consider the composition of magnesiowüstite immediately adjacent to the interface with Fe to be the composition in local equilibrium with the liquid metal [e.g., *O'Neill et al.*, 1998; *Asahara et al.*, 2007].

3.1.3. Oxygen in Quenched Liquid Iron

[12] As described in section 2.1, after chemical mapping the samples were rethinned with an argon ion-beam milling system. Then quantitative analysis of oxygen in the quenched iron was conducted using EELS. A representative EELS spectrum is shown in Figure 5. The maximum oxygen concentration in quenched iron determined in our experiments was about 32.5 mol% in the sample from the experiment performed at 70 GPa and 3500 K (sample M95I70). In this sample, the oxygen concentrations in the observed area of quenched liquid iron (about 1 μm × 1 μm) varied from 13 to 32.5 mol% (using a beam diameter of 100 nm). Such a large variation was observed only in the sample M95I70, and in other samples the compositions were relatively homogeneous. We assume that the average of such measurements gives the oxygen concentration of the liquid iron. The averages and standard deviations of the measurements are listed in Table 2.

[13] Quenched liquid iron consisted mainly of polycrystalline α-iron, but some undefined diffraction spots were observed in addition to those of α-iron in samples with high-oxygen concentrations. Wüstite is a possible candidate for this minor phase, though this is difficult to confirm on the basis of a few diffraction spots. Heterogeneity in oxygen concentrations apparent in some quenched iron veins is most likely caused by the presence of an FeO phase that exsolved during quenching [cf, *O'Neill et al.*, 1998; *Gessmann and Rubie*, 1998]. At the interface between magnesiowüstite and quenched Fe, magnesioferrite was also observed on the basis of minor diffraction spots in sample M95I70 (see Figure 6). It is, therefore, suggested that part of the exsolved FeO component reacted with magnesiowüstite at the metal-oxide interface during the quench. A similar reaction was reported by *O'Neill et al.* [1998] in multianvil experiments.

[14] Experimental results are shown in Figure 7 and compared with the model of *Asahara et al.* [2007]. The model of *Asahara et al.* [2007] is based on the assumption that K_D varies only as a function of P and T and was constrained using multianvil data to 25 GPa and estimates for K_D determined from DAC studies on oxygen partitioning between liquid Fe and silicate perovskite at higher pressures [*Takafuji et al.*, 2005; *Sakai et al.*, 2006]. The metal-magnesiowüstite K_D was estimated from the latter studies using data on Fe-Mg partitioning between silicate perovskite and magnesiowüstite. Even though the uncertainties in the experimental data determined in this study are large, the data are still in quite poor agreement with the model proposed by *Asahara et al.* [2007] as only one of the data points at 3100 K (M98I65) is consistent with this model. The K_D values from this study are also consistently higher than the experimental data of *Ozawa et al.* [2008].

3.1.4. Carbon Contamination in the Sample

[15] Contamination by carbon was observed in a sample recovered from an experiment at 72 GPa and 3200 K (run no. M95I70_02, not reported in Table 1). Fe-rich veins have a granular texture and consist of FeO and Fe_7C_3 (Figure 8). We examined the carbon distribution in all sample foils using STEM mapping, and we normally found a homogeneous distribution that resulted from the sample being coated with carbon for TEM observations (see Figure 3e). However, in this sample, we could clearly observe high concentrations of carbon in the metal using STEM mapping.

Table 2. Run Products of Fe-FeO Liquidus Experiments

Run	Pressure (GPa)	T (K)	OEL/TEL[a]	Starting Composition (mol%)	Fe-Rich Liquid		FeO-Rich Liquid	
					FeO (mol%)	Fe (mol%)	FeO (mol%)	Fe (mol%)
FO07	24.5	2473	10/4	34	35(7)	64(14)	53(9)	47(8)
				18	35(6)	64(12)		
				18	31(8)	68(18)		
FO06	20	2473	10/5	34	19(2)	81(8)	62(3)	38(1)
				18	15(2)	85(12)		
FO05	12	2373	10/5	18	8.4(1)	91(1)	95(6)	5.2(3)
				34	6(1)	93(1)	85(13)	15(2)

[a]OEL is the octahedral edge length of the MgO pressure medium, and TEL is the truncation edge length of the tungsten carbide cubes.

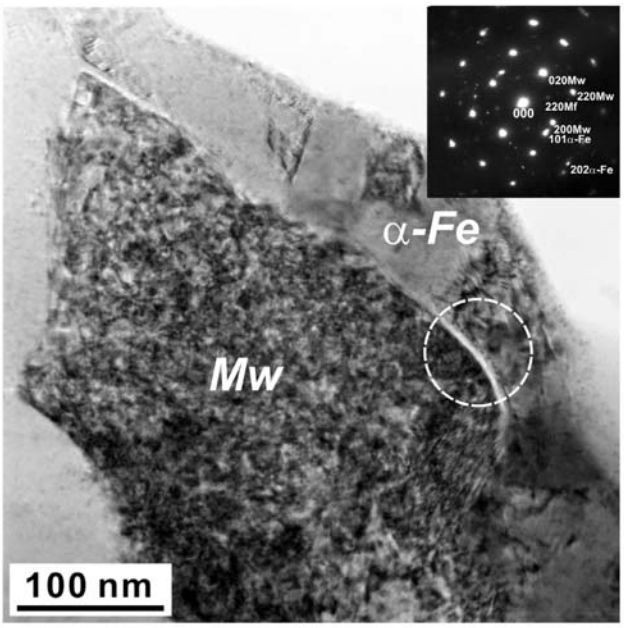

Figure 6. Bright field transmission electron micrograph of iron and adjacent magnesiowüstite in the sample foil from the sample reacted at 70 GPa and 3500 K (run: M95I70). The selected area electron diffraction pattern shown in the insert was obtained from the area indicated by the white dashed circle. The main diffraction spots are from α-iron and magnesiowüstite (Mw) but additional spots are present that can be indexed as magnesioferrite (Mf, spinel structure).

On the basis of this unique result, we consider that carbon contamination occurred in this sample at least in the analyzed regions. Graphite inclusions in the magnesiowüstite starting material or chemical reaction between the sample and diamond [*Dubrovinsky et al.*, 2005] are possible origins of this contamination. We excluded this sample from further consideration.

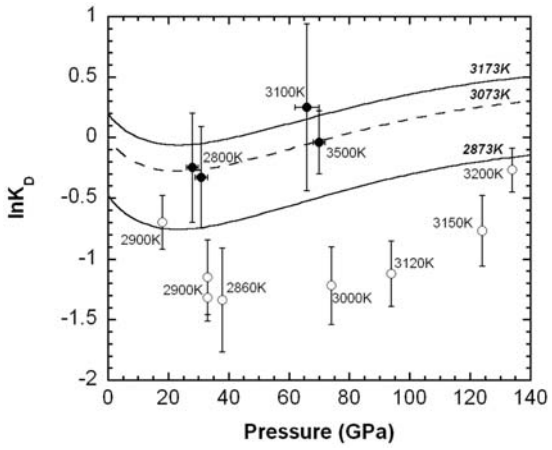

Figure 7. The experimentally determined values of ln K_D obtained by LHDAC experiments in this study and by *Ozawa et al.* [2008] are compared with the thermodynamic model previously reported by *Asahara et al.* [2007]. Data from this study and *Ozawa et al.* [2008] are shown by filled and open circles, respectively, and are labeled with the experimental temperatures. The curves show the model of *Asahara et al.* [2007] calculated at temperatures indicated next to each curve.

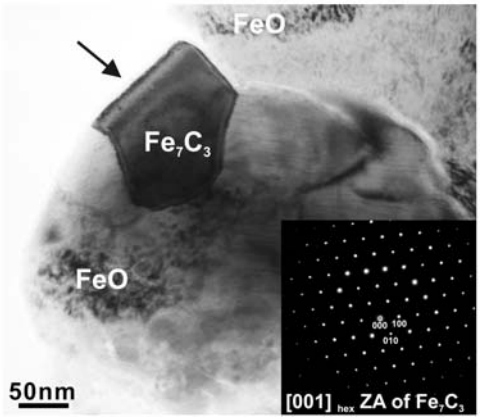

Figure 8. Bright field transmission electron micrograph of a metallic vein in the sample that was reacted at 71 GPa and 3200 K (run: M95I70_02). The selected area electron diffraction (SAED) pattern inserted in the figure was obtained from the grain indicated by the arrow. It is identified as a Fe_7C_3 phase with hexagonal or orthorhombic symmetry [*Yakel*, 1985]. The SAED pattern was indexed with the hexagonal symmetry.

3.2. Multianvil Fe-O Liquid Immiscibility Experiments

[16] Metallic iron-rich liquids and ionic iron oxide-rich liquids both quenched to an assemblage containing quenched crystals of iron and iron oxide phases. In many samples, however, it was possible to identify the presence of immiscible liquids through the occurrence of clear compositional boundaries as shown in Figure 9. The results show that the oxygen content of liquid Fe metal in equilibrium with FeO-rich ionic liquid increases relatively strongly with pressure, while, in comparison, the oxygen content of the coexisting ionic liquid decreases to a slightly smaller extent with pressure. The results shown in Figure 10 are in good agreement with coexisting liquid compositions reported by *Tsuno et al.* [2007], which were collected between 2173 and 2573 K at 15, 18, and 21 GPa. The data of *Tsuno et al.* [2007] also indicate that the immiscible region closes with increasing temperature. At 24.5 GPa, the difference in the oxygen contents of metallic and ionic liquids is approximately 10 mol%.

4. Thermodynamic Analysis

4.1. Fe-O System

[17] Using the high-temperature oxygen solubility data of *Fischer and Schumacher* [1978] and *Distin et al.* [1970], *Kowalski and Spencer* [1995] derived a thermodynamic model that describes liquid immiscibility in the Fe-O system at ambient pressure. The associated solution model employs Fe, FeO, and $FeO_{1.5}$ liquid species and predicts closure of the miscibility gap between Fe-rich metallic and FeO-rich ionic liquids at approximately 3000 K. The species have strong nonideal interactions in the liquid, but above 2000 K the proportion of $FeO_{1.5}$ species in the ionic liquid predicted by the model is small (<5 mol%), and a very minor shift in

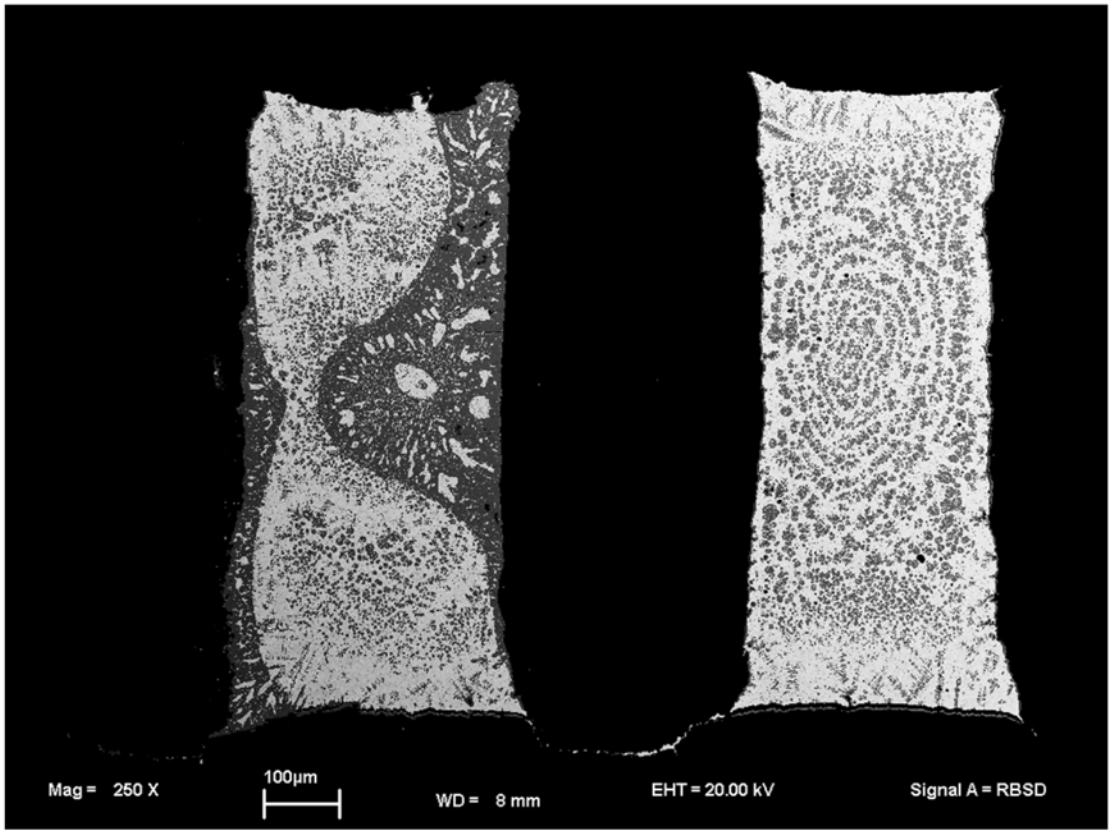

Figure 9. Scanning electron microscope image of two samples contained in a single alumina capsule from an experiment performed in the Fe-FeO system at 20 GPa and 2473 K. The sample on the left with a starting material of Fe with 9 wt% O contains coexisting metal and ionic liquids, while that on the right (5 wt% O) is interpreted to consist of a single metallic liquid. When quenched, both metallic and ionic liquids crystallize to mixtures of Fe and FeO.

liquid compositions results if $FeO_{1.5}$ species are ignored. This makes the model computationally much simpler as the two liquids at equilibrium are then described using two chemical potentials, one for each component:

$$\mu_{\mathrm{Fe}}^{\mathrm{metallic}} = \mu_{\mathrm{Fe}}^{\mathrm{ionic}}, \tag{2}$$

$$\mu_{\mathrm{FeO}}^{\mathrm{metallic}} = \mu_{\mathrm{FeO}}^{\mathrm{ionic}}. \tag{3}$$

Taking the standard state as the pure phases at the pressure and temperature of interest, the expressions for the chemical potentials of FeO in the metallic and ionic phases are

$$\mu_{\mathrm{FeO}}^{\mathrm{metallic}} = \mu_{\mathrm{FeO},P,T}^{\bigcirc,\mathrm{metal}} + RT\ln X_{\mathrm{FeO}}^{\mathrm{metal}} + RT\ln\gamma_{\mathrm{FeO}}^{\mathrm{metal}}, \tag{4}$$

$$\mu_{\mathrm{FeO}}^{\mathrm{ionic}} = \mu_{\mathrm{FeO},P,T}^{\bigcirc,\mathrm{ionic}} + RT\ln X_{\mathrm{FeO}}^{\mathrm{ionic}} + RT\ln\gamma_{\mathrm{FeO}}^{\mathrm{ionic}}, \tag{5}$$

where $\mu_{\mathrm{Feo},P,T}^{\bigcirc}$ is the standard state chemical potential, R is the gas constant and $\gamma_{\mathrm{FeO}}^{\mathrm{metal}}$ is, for example, the activity coefficient of FeO in the metallic phase. Similar equations can be written for the Fe components in the two liquid phases. When component chemical potentials are equated, as in equation (3), the standard state terms cancel out and can therefore be ignored for the present. The nonideal mixing terms for FeO and Fe in both metallic and ionic liquids are described using asymmetric Margules equations

$$RT\ln\gamma_{\mathrm{FeO}} = (1 - X_{\mathrm{FeO}})^2[W_{\mathrm{FeO-Fe}} + 2(W_{\mathrm{Fe-FeO}} - W_{\mathrm{FeO-Fe}})X_{\mathrm{FeO}}], \tag{6}$$

and

$$RT\ln\gamma_{\mathrm{Fe}} = (1 - X_{\mathrm{Fe}})^2[W_{\mathrm{Fe-FeO}} + 2(W_{\mathrm{FeO-Fe}} - W_{\mathrm{Fe-FeO}})X_{\mathrm{Fe}}], \tag{7}$$

where $W_{\mathrm{FeO\text{-}Fe}}$ and $W_{\mathrm{Fe\text{-}FeO}}$ are interaction parameters. At ambient pressure, these terms are a function of temperature but in order to fit the high-pressure data a pressure-dependent term, i.e., an excess volume, is also included. Using a least-squares fitting routine, we derive two excess volume terms from the high-pressure experimental data to give

$$W_{\mathrm{FeO-Fe}} = 135,943 - 31.122T - 0.059(6)P, \tag{8}$$

and

$$W_{\mathrm{Fe-FeO}} = 83,307 - 8.978T - 0.09(2)P, \tag{9}$$

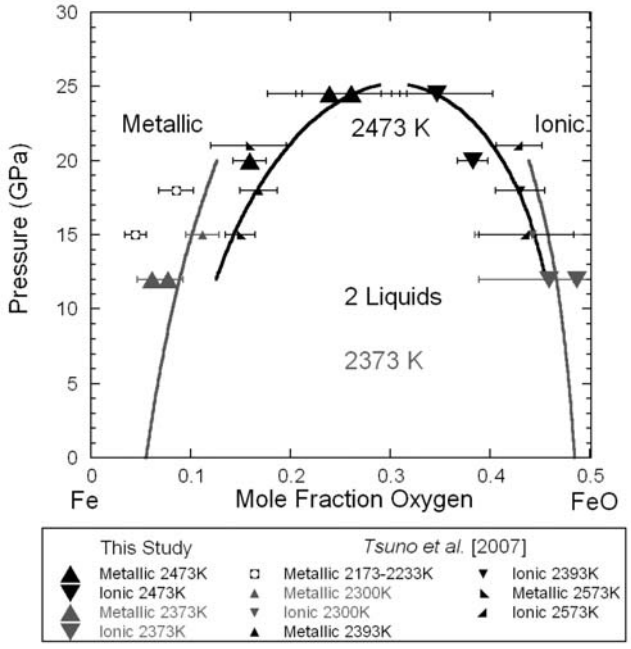

Figure 10. Compositions of coexisting Fe and FeO-rich liquids from high-pressure experiments at 2373 and 2473 K in the Fe-FeO system. Previous data from *Tsuno et al.* [2007] are shown for comparison. The thermodynamic calculation of the miscibility gap derived from the experimental data obtained in this study is shown at 2373 K (gray line) and 2473 K (black line).

where the pressure P is in bars. The first two terms in each expression are derived from the ambient pressure Redlich-Kister expressions given by *Kowalski and Spencer* [1995], and the final term, related to the excess volume, is derived from the high-pressure data. The uncertainties in the excess volume terms are derived from the standard deviation of individual fits to the miscibility gap at each pressure. The uncertainty in the $W_{\text{Fe-FeO}}$ excess volume is quite large mainly as a result of the data at 12 GPa. As will be seen, however, the effect of this uncertainty on the calculations described in section 5 is relatively small. The fit of this model to the high-pressure data is shown in Figure 10. Although the model was refined using only the data from this study, its predictions are also in good agreement with the coexisting liquid compositions reported by *Tsuno et al.* [2007].

4.2. Mg-Fe-O System

[18] In order to calculate the oxygen content of liquid iron metal in equilibrium with magnesiowüstite of a given FeO content, we need to consider the equilibrium between the FeO components, i.e.,

$$\mu_{\text{FeO}}^{\text{metal}} = \mu_{\text{FeO}}^{\text{magnesiowustite}}. \tag{10}$$

The chemical potentials for each phase are given by equations (4) and (5), where magnesiowüstite now takes the place of the ionic liquid. Although samples of magnesiowüstite are generally nonstoichiometric to some extent as a result of the presence of $FeO_{1.5}$ defects, experiments have shown that samples synthesized under high pressures have significantly lower $FeO_{1.5}$ contents than at ambient pressures [*McCammon*, 1993]. In the development of the following model, we, therefore, assume magnesiowüstite to be stoichiometric. Activity-composition relations for FeO in the metallic phase are given by equations (6)–(9) and for magnesiowüstite a symmetric solution model is employed from the literature [*O'Neill et al.*, 2003; *Frost*, 2003]:

$$RT \ln \gamma_{\text{FeO}}^{\text{mw}} = (1 - X_{\text{FeO}}^{\text{mw}})^2 W_{\text{FeO-MgO}}^{\text{mw}}, \tag{11}$$

with

$$W_{\text{FeO-MgO}}^{\text{mw}} = 11,000 + 0.011P \ \ (\text{bars}). \tag{12}$$

As opposed to the Fe-O system, the standard state chemical potentials of FeO in liquid Fe and magnesiowüstite no longer cancel out across equilibrium (10) but can be determined using thermodynamic data extracted from the melting curve of FeO. The chemical potential of solid FeO was determined from room pressure free energy data [*Kowalski and Spencer*, 1995] and using *P-V-T* equation of state data from high-pressure measurements [*Seagle et al.*, 2008]. The chemical potential of liquid FeO was then determined at high pressure and temperature by refining a *P-V-T* equation of state for the liquid using data on the melting curve of FeO. Data from *Lindsley* [1966], *Tsuno et al.* [2007], and *Seagle et al.* [2008] were employed to fit the melting curve. The high-pressure results of *Seagle et al.* [2008] were preferred over other studies because they bracket the melting temperature of a composition that is close to stoichiometric FeO. In the refinement of the equation of state properties of liquid FeO, the experimental melting data were weighted using the temperature uncertainties. The refined melting curve is shown in Figure 11. The thermodynamic parameters for the fit are reported in Table 3. It may not be possible to use the FeO melting curve to determine the chemical potential of FeO liquid relative to the cubic FeO end member at pressures above 70 GPa because cubic FeO goes through a phase transformation to the NiAs-type B8 structure [*Fei and Mao*, 1994], which may appear on the solidus above 70 GPa.

[19] The proportion of FeO in Fe liquid at a given P, T, and magnesiowüstite Fe/(Fe + Mg) can be calculated using equation (10) and employing equations (4)–(12) to calculate the chemical potential of FeO in each phase. The oxygen distribution coefficient (K_D) can then be calculated using the determined FeO contents. In Figure 12, curves calculated for K_D using this model are compared with the multianvil experimental data of *Asahara et al.* [2007]. The curves are calculated for a magnesiowüstite Fe/(Fe + Mg) ratio of 0.15, which is midway within the range of values displayed by the experimental data. The model curves are in excellent agreement with the experimental data, although the model was derived completely independently.

[20] In Figure 13a, the thermodynamic model is compared with the DAC results obtained in this study. The model curves are calculated for the magnesiowüstite compositions of the individual experiments. At pressures below 25 GPa, the model predicts that K_D is independent of

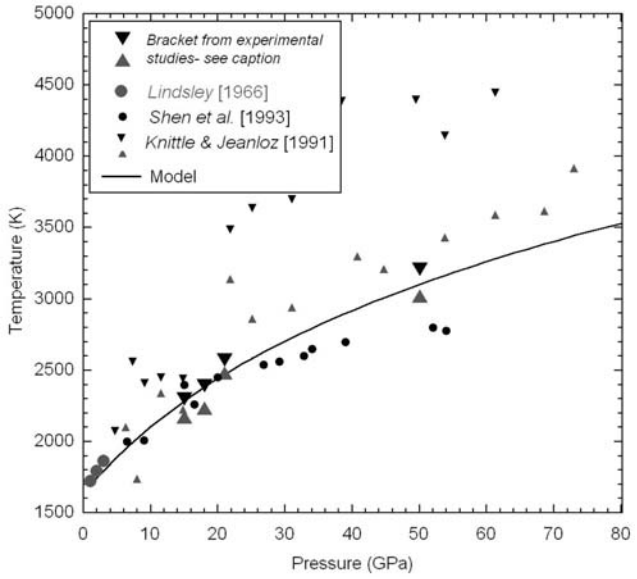

Figure 11. Experimental determinations of the melting curve of Fe_xO. The model (solid black curve) has been derived by fitting the *P-V-T* properties of liquid FeO using the experimental data of *Lindsley* [1966] up to 3 GPa, *Tsuno et al.* [2007] up to 20 GPa and *Seagle et al.* [2008] at 50 GPa, (with the experimental brackets provided by the latter two studies indicated by filled and shaded large opposed triangles). The standard state chemical potential of liquid FeO is obtained at high pressure and temperature using the fitted melting curve and thermodynamic properties of solid Fe_xO.

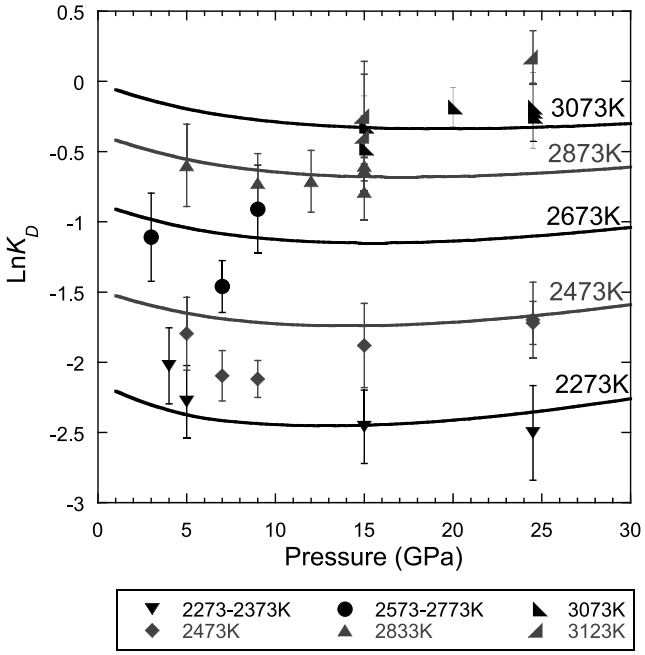

Figure 12. Oxygen distribution coefficients (K_D) calculated with the thermodynamic model described in the text (solid curves) are compared with the multianvil experimental data of *Asahara et al.* [2007].

composition. However, above 25 GPa, K_D becomes strongly dependent on the magnesiowüstite FeO content. As shown in Figure 13a, above 25 GPa the curve calculated at 3500 K for a magnesiowüstite Fe/(Fe + Mg) ratio of 0.19 flattens out and crosses beneath that calculated for a lower temperature and lower magnesiowüstite Fe content. This behavior is mirrored exactly by the experimental data, with which the model is in excellent agreement, even though it has been derived completely independently.

[21] Data from the recent study of *Ozawa et al.* [2008], which was performed up to 134 GPa, are also shown up to 80 GPa in Figure 13a. Between 18 and 94 GPa, values of ln K_D determined by *Ozawa et al.* [2008] are consistently lower by up to 1 natural log unit compared with our model, although data at 134 and 124 GPa are within 0.3 natural log units of the model, which is close to the reported experimental uncertainty. The lower Fe metal oxygen contents and consequent low values of K_D reported by *Ozawa et al.* [2008] could have resulted from FeO loss from Fe-liquid during quenching, as observed in previous studies by *O'Neill et al.* [1998]. As the Fe liquid metal cools during quenching, FeO liquid exsolves and can migrate to the boundary with the surrounding magnesiowüstite. If samples quench too slowly or Fe liquid regions are relatively small, the time scale for this process can be short enough for the Fe to be strongly depleted in FeO. On the other hand, unless temperatures in our study were significantly overestimated,

Table 3. Thermodynamic Model Parameters[a]

Parameter	Value	Reference[b]
FeO solid		
$\mu^\circ_{(\text{Wüstite,1 bar,T})}$ (kJ mol^{-1})	$-279318 + 252.848T - 46.12826T\ln(T) - 0.00574029 84T^2$	1
$V_{0,298\text{K}}$ (J/bar)	1.225	2
α, thermal expansion (K^{-1})	$3.481e^{-5} + 2.968e^{-9}T - 0.0806T^{-2} - 0.0014437T^{-1}$	2
K_T (bar)	$1{,}500{,}000 - 2.64e^2(T\text{-}298) + 0.01906(T\text{-}298)^2$	3
K'	4.305	3
FeO liquid		
$\mu^\circ_{(\text{FeO,liquid,1 bar,T})}$ (kJ mol^{-1})	$\mu^\circ_{(\text{Wüstite,T,1 bar,})} + 34{,}008 - 20.969T$	1
$V_{0,298\text{ K}}$ (J/bar)	1.3244	4
α, thermal expansion (K^{-1})	$4.923e^{-5} + 2.968e^{-9}T - 0.0806T^{-2} - 0.0014437T^{-1}$	4
K_T (bar)	$802{,}655 - 100(T\text{-}298)$	4
K'	4.397	4

[a]The chemical potential of each phase at the P and T of interest is calculated from $\mu(P, T) = \mu^\circ(1\text{ bar}, T) + \int_1^P V_{\text{FeO}}\,dP$, where $\int_1^P V_{\text{FeO}}\,dP = V_T\{K_T/(K' - 1)*[(1 + K'/K_T\text{P})^{((K'-1)/K')} - 1]\}$, and $V_T = V_{0,298}\exp[\int_{298}^T \alpha dT]$.

[b]References: 1, *Kowalski and Spencer* [1995]; 2, *Hass and Hemingway* [1992]; 3, refined from the data of *Seagle et al.* [2008]; 4, refined from the FeO melting curve.

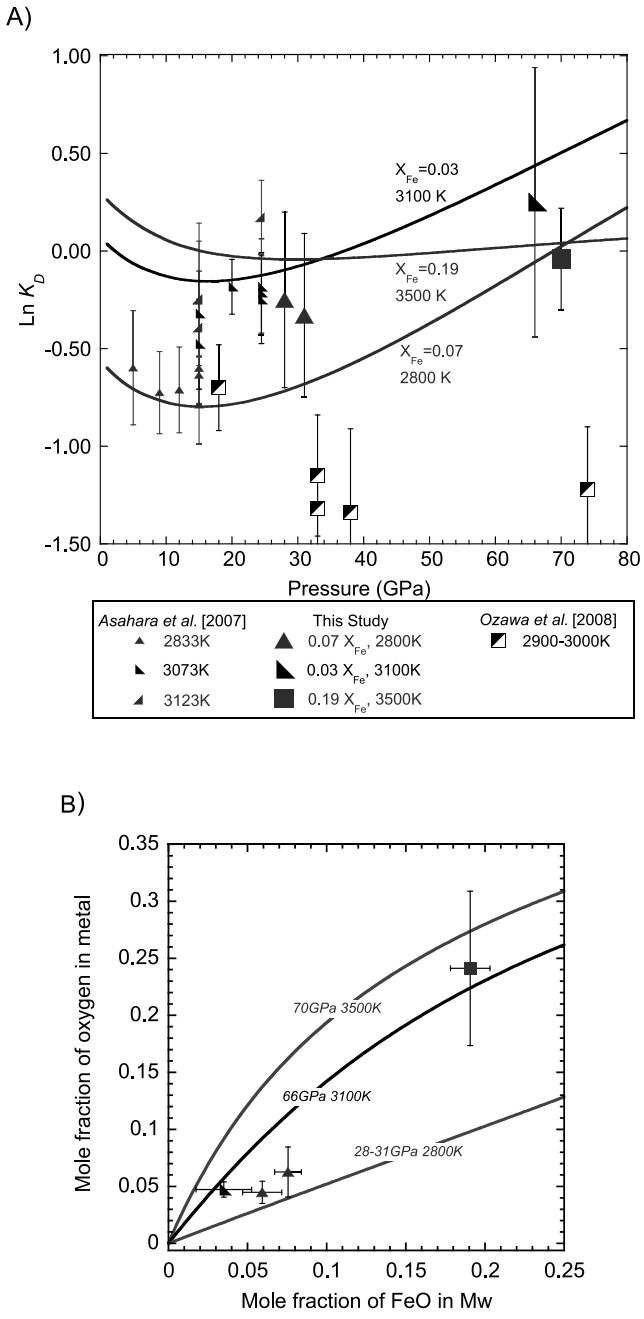

Figure 13. (a) Results of oxygen partitioning experiments from the diamond anvil cell between 28 and 70 GPa are compared with curves calculated from the thermodynamic model for the individual experimentally observed magnesiowüstite Fe/(Fe + Mg) values (XFe). At high pressure, the model predicts that K_D becomes compositionally dependent, in good agreement with the experimental data. Data from the recent study of *Ozawa et al.* [2008] are also shown. (b) The oxygen content of liquid Fe metal in the experimental samples is plotted as a function of the equilibrium magnesiowüstite Fe/(Fe + Mg) ratio. Curves calculated at the experimental pressures and temperatures are determined from the thermodynamic model. Symbols are the same as those in Figure 13a. At high pressure, the curves are no longer linear, indicating that K_D is no longer constant with varying magnesiowüstite Fe/(Fe + Mg).

it is hard to envisage experimental mechanisms that could lead to erroneously high values of K_D.

[22] In Figure 13b, the Fe metal oxygen concentration has been calculated as a function of the FeO content of magnesiowüstite at the conditions of our experiments using the thermodynamic model. The experimental data are also plotted. At low pressure, there is a linear relationship and K_D, which is essentially the gradient, is constant with composition. A curvature develops at high pressures and temperature, however, causing K_D, to become compositionally dependent. Models that assume a constant K_D will therefore tend to overestimate oxygen concentrations at typical FeO concentrations and conditions of the present-day lower mantle.

[23] The predictions of the model, particularly when extrapolated to the core-mantle boundary, are sensitive to the melting curve of FeO employed. We use a melting curve constrained by the data of *Seagle et al.* [2008]; however, previous experimental studies by *Shen et al.* [1993] and *Knittle and Jeanloz* [1991] have derived both lower and higher temperature melting curves, respectively (Figure 11). Some idea of the uncertainties in the model can also be gained by employing these two studies to calibrate the model. When using the data of *Shen et al.* [1993], a relatively minor shift in the calculated ln K_D occurs with values that are on average more positive by approximately 0.5 natural log units at 60 GPa. Although still generally consistent with our diamond cell results, a poorer fit is obtained. When employing a curve that is bracketed midway between the liquid and solid temperatures reported by *Knittle and Jeanloz* [1991] values of ln K_D are driven consistently lower with pressure and the minima apparent for low X_{Fe} compositions in Figure 13 disappears. At 60 GPa, the calculated ln K_D is approximately 0.8 log units below the curve at 3100 K shown in Figure 13a and is, therefore, in poor agreement with our experimental data. This model is in much better agreement with the data of *Ozawa et al.* [2008] up to pressures of 74 GPa, but because the model displays no minima it predicts values that are over 1 natural log unit lower than the experimental data of *Ozawa et al.* [2008] at the highest reported pressure (134 GPa). There is, however, a large difference in temperature between conditions where the solid and liquid phases are observed in the study of *Knittle and Jeanloz* [1991], and a melting curve passing closer to the minimum estimated temperature up to 70 GPa would be quite consistent with the results of *Seagle et al.* [2008], and multianvil experiments [*Tsuno et al.*, 2007] and result in an oxygen partitioning model that is very similar to that shown in Figure 13.

5. Discussion

[24] Using the equation of state for FeO liquid and the determination of the excess volume of mixing between Fe and FeO liquids, we can make an estimate of the amount of oxygen required to satisfy the density deficit of the outer core. Comparing the density of pure liquid iron [*Alfè et al.*, 2002b] with the PREM model [*Dziewonski and Anderson*, 1981] at 5000 K and 150 GPa implies that the core has a 9% density deficit. Extrapolating our FeO liquid equation of state to the same conditions and employing the excess volume of mixing indicates that 6 wt% oxygen would be

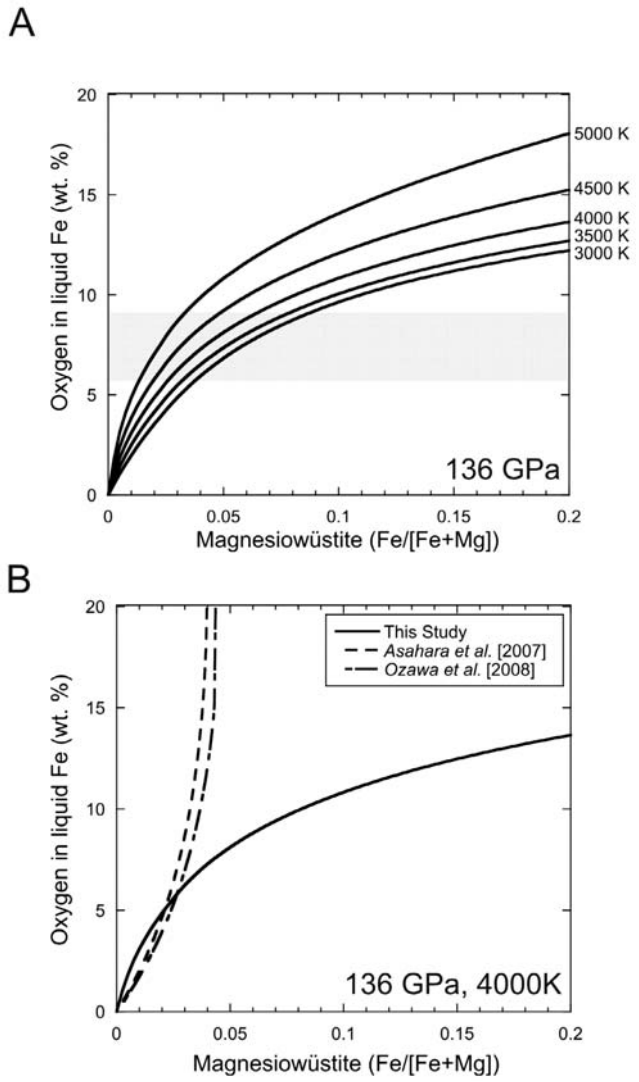

Figure 14. (a) The oxygen content of liquid Fe metal versus the equilibrium magnesiowüstite Fe/(Fe + Mg) calculated at the present-day core-mantle boundary pressure of 136 GPa between 3000 and 5000 K. The temperature at the core-mantle boundary is likely in the range 3500–4500 K. The shaded region indicates the range of oxygen contents required to account exclusively for the density deficit of the outer core. Magnesiowüstite FeO contents in equilibrium with plausible core oxygen contents are much lower than those expected for the bulk of the mantle, showing that either the mantle adjacent to the outer core must be depleted in FeO or that a stratified outer layer of the core must be enriched in oxygen. (b) The oxygen content of liquid Fe calculated with the thermodynamic model developed in this study is compared with the previous models of *Asahara et al.* [2007] and *Ozawa et al.* [2008] for which it was assumed that K_D is independent of magnesiowüstite composition.

required to cause this density deficit, if oxygen is the only light element in the core. This is in good agreement with previous estimates [*Alfè et al.*, 2002a], which at the very least serves to show that our equation of state for FeO liquid is consistent with determinations made through more sophisticated methods. Accounting for the negative excess volume of mixing between Fe and FeO decreases the amount of O required to satisfying the density deficit by approximately 0.5 wt%.

[25] At low pressures, Fe-FeO immiscibility is reflected in large positive deviations from ideality of the Fe-FeO liquids. The negative excess volume of mixing drives activities toward ideal mixing with increasing pressures, but by core-mantle boundary (CMB) pressures this causes negative deviations from ideality to develop. While we cannot assess the effects of pressure on the excess volumes, we note that such negative deviations imply the presence of ordered intermediate liquid species such as Fe_2O. This could be an indication that corresponding solid phases with similar stoichiometries may also become stable at these conditions, although to date none have been identified.

[26] By extrapolating the model to conditions of the present-day CMB (136 GPa), the relationship between the oxygen content of the core and the Fe/(Fe + Mg) of magnesiowüstite at the CMB can be determined. Estimates for the temperature at the CMB range between 3500 and 4500 K, and the oxygen content of the core would need to be in the range of 6–9 wt%, if oxygen is the sole cause of the core's density deficit. The range reflects the uncertainties in both the density of the core and the effect of oxygen on the density of Fe. As shown in Figure 14a, these ranges of temperature and oxygen content correspond to a range in magnesiowüstite Fe/(Fe + Mg) of 0.02–0.08, which is below that expected for the bulk of the mantle (Fe/(Fe + Mg) = 0.12) even if the favorable partitioning of FeO into magnesiowüstite over all other silicate phases is ignored [*Wood*, 2000; *Kesson et al.*, 1998; *Murakami et al.*, 2005]. Therefore, even if oxygen is the sole light element in the core, the core must be undersaturated in oxygen with respect to the likely mantle FeO concentration. The mantle at the CMB might, therefore, become strongly depleted in FeO in order to achieve local equilibrium with the core. If oxygen is not the only light element in the core or if it is only a minor component, then an even stronger depletion of FeO from the mantle could develop. On the other hand, instead of the base of the mantle becoming depleted in FeO, it is also possible that the core has developed a low-density, dynamically stable FeO-rich outer layer, as a result of reaction with the mantle. Seismic studies have proposed evidence for a layer on top of the outer core of the order of 10 km thick [*Eaton and Kendall*, 2006; *Tanaka*, 2007]. As the core cooled, the mantle at the CMB might even have become enriched in FeO as a result of backreaction with this outer core layer. Although not mutually exclusive, whether chemical equilibrium at the CMB is achieved through FeO depletion of the mantle or FeO enrichment of a layer at the top of the core will depend on the dynamics of mixing in the mantle and core. A well-mixed core will favor the former possibility, while effective mixing of the mantle will favor the latter.

[27] There are significant uncertainties in the model inherent in the extrapolation to the CMB and in the use of a simplified chemical system. The uncertainty in the determined Fe-FeO excess volume, for example, propagates to an uncertainty in the calculated core oxygen contents shown in Figure 14 of approximately 1 wt% oxygen. It is possible that structural changes in Fe liquid affect Fe-FeO excess

properties at pressures above 25 GPa, which would invalidate our simple extrapolation. Other than the consistency between our model and experimental partitioning data up to 60 GPa, we have no way to assess this possibility. As discussed in section 4.2, use of different melting curves for FeO can also have a strong influence on the model. If the melting curve of *Shen et al.* [1993] is employed, for example, the curves shown in Figure 14 shift to much higher oxygen concentrations and the core is, therefore, predicted to be even more undersaturated in oxygen. If the FeO melting curve is derived from the midpoint of the data reported by *Knittle and Jeanloz* [1991], on the other hand, very little oxygen is predicted to dissolve in the core at current CMB conditions. The excellent agreement between our model and the diamond anvil cell results, however, is strong support for our choice of the FeO melting curve of *Seagle et al.* [2008].

[28] In our experiments, we have ignored the effects of Ni and other potential light elements in the core. It is possible that ternary interactions between other light elements such as sulfur and silicon could strongly affect oxygen partitioning between the mantle and core. Some inconsistencies between the studies of *Rubie et al.* [2004] and *Asahara et al.* [2007], for example, might be explained by the presence of Ni and Si in the liquid Fe in the former study. These possibilities await detailed investigation.

[29] The strong compositional dependence of oxygen partitioning that develops at high pressures is compared with previous models at 136 GPa and 4000 K in Figure 14b. The studies of *Asahara et al.* [2007] and *Ozawa et al.* [2008] assumed that the oxygen K_D remains constant with magnesiowüstite composition, and the resulting curves for the liquid-metal oxygen content become very steep at CMB conditions, predicting metal oxygen contents above 20 wt% for magnesiowüstite Fe/(Fe + Mg) < 0.05 at 4000 K. On the basis of these earlier models, significant core-mantle equilibration at the base of a magma ocean that extended significantly into the deep lower mantle would be ruled out on the grounds that this would have left the mantle strongly depleted in FeO because of oxygen partitioning into the core [*Frost et al.*, 2008]. With the current model, however, significant core-mantle equilibration at conditions compatible with the base of a magma ocean in the lower portion of the lower mantle cannot be ruled out. On the other hand, simple single-stage homogeneous accretion calculations indicate that for oxygen to be the major light element in the core, core-mantle equilibration would have had to occur predominantly at the base of a magma ocean that extended to a depth where pressures reached at least 70 GPa. The Earth would also have had to form from material that was at least as oxidized as the present-day mantle.

6. Conclusions

[30] Oxygen partitioning experiments between magnesiowüstite and liquid iron have been performed up to 70 GPa and 3500 K with the LHDAC. An FIB-milling technique was employed to prepare thin foils from the recovered samples for chemical analysis with the TEM. Partitioning data obtained in this study are in good agreement with previous data obtained using the multianvil apparatus up to 25 GPa. The results, however, suggest that the oxygen distribution coefficient, K_D, is not independent of the magnesiowüstite FeO content over the ranges of FeO concentration investigated at pressures >25 GPa. This must result from changes in the excess free energy properties, i.e., activity composition relations, for the liquid and oxide phases with increasing P and T. The existing partitioning data are insufficient to accurately calibrate this compositional effect, however.

[31] Further experiments were performed to independently derive the excess free energy properties of Fe-FeO liquids. Compositions of immiscible Fe and FeO-rich liquids were determined up to 25 GPa at 2373–2473 K. The miscibility gap was found to close with increasing P and T, in good agreement with the previous study of *Tsuno et al.* [2007]. A thermodynamic model fit to these data allowed the activity of FeO in Fe liquid to be calculated as a function of P and T. A small, negative excess volume of mixing between FeO and Fe liquids was found. In order to construct a model to describe oxygen partitioning in the Mg-Fe-O system at high P and T, three further forms of data were employed.

[32] 1. Activity-composition relations for the magnesiowüstite solid solution were taken from the literature.

[33] 2. The chemical potential of pure FeO in magnesiowüstite was determined using room temperature free energy data and P-V-T equation of state data from the literature.

[34] 3. The chemical potential of pure FeO in liquid metal was determined by fitting high-pressure experimental data on the melting curve of FeO.

[35] The resulting model reproduces both multianvil oxygen partitioning data to 25 GPa and the LHDAC experimental results obtained in this study. The independent method by which this model was determined provides rigorous confirmation of the trends indicated by the experiments. The model shows that the oxygen K_D, while being independent of magnesiowüstite composition at pressures <25 GPa, becomes a strong function of composition at higher pressures, in agreement with the experimental data.

[36] Extrapolating the model to calculate the effect of FeO on the density of the outer core indicates that 6 wt% oxygen would be required to explain the core density deficit, which is in agreement with previous studies [*Alfè et al.*, 2002a]. The core could contain this level of oxygen as a result of core-mantle equilibration in a terrestrial magma ocean [*Asahara et al.*, 2007; *Rubie et al.*, 2007; *Frost et al.*, 2008]. The strong compositional dependence of oxygen partitioning that occurs at high pressures, however, means that the mantle would not have been drastically depleted in FeO as a result of such equilibration, as predicted by some previous models, even if the magma ocean extended deep into the lower mantle.

[37] As discussed by *Asahara et al.* [2007], if the compositions of Earth's mantle and core were established through magma ocean equilibration, then, at the present-day CMB, the core will be oxygen undersaturated with respect to the likely mantle magnesiowüstite composition of Fe/(Fe + Mg) = 0.12–0.18 [*Kesson et al.*, 1998; *Wood*, 2000; *Murakami et al.*, 2005]. As a result the mantle might be locally depleted in FeO at the CMB due to partitioning into the core, in order that the mantle and core can attain local equilibrium. The resulting MgO-rich layer at the CMB might be very thin because Fe-Mg diffusion, at least in silicate perovskite, is extremely slow at these conditions [*Holzapfel et al.*, 2005]. Alternatively, FeO extracted from

the mantle could have concentrated in a dynamically stable FeO-rich layer at the top of the outer core. It is, therefore, possible that layering develops on both sides of the CMB, with extents and compositions that depend on the dynamics of mixing on either side. It is quite likely that, in addition to oxygen, the core contains several other light elements, such as Si and S. Further studies are required in order to constrain the effects of these elements on oxygen partitioning.

[38] **Acknowledgments.** We thank Hubert Schulze for sample preparation and Christian Liebscher and Uwe Glatzel for their help with TEM observations. Y.A. was partially supported by a JSPS Research Fellowship for young scientists. This study was partly funded by the German Science Foundation Priority Program "Mars and the Terrestrial Planets" (Ru 437/6-2) and was partially carried out under the Visiting Researcher's Program of the Institute for Study of the Earth's Interior, Okayama University. Denis Andrault is thanked for constructive comments on an early version of this manuscript, and the manuscript was further improved by the comments and suggestions of two anonymous reviewers.

References

Alfè, D., M. J. Gillan, and G. D. Price (2002a), Composition and temperature of the Earth's core constrained by combining ab initio calculations and seismic data, *Earth Planet. Sci. Lett.*, *195*, 91–98, doi:10.1016/S0012-821X(01)00568-4.

Alfè, D., G. D. Price, and M. J. Gillan (2002b), Iron under Earth's core conditions: Liquid state thermodynamics and high-pressure melting curve from ab initio calculations, *Phys. Rev. B*, *65*, 165118, doi:10.1103/PhysRevB.65.165118.

Asahara, Y., D. J. Frost, and D. C. Rubie (2007), Partitioning between magnesiowüstite and liquid iron at high pressures and temperatures: Implications for the composition of the Earth's outer core, *Earth Planet. Sci. Lett.*, *257*, 435–449, doi:10.1016/j.epsl.2007.03.006.

Birch, F. (1952), Elasticity and constitution of the Earth's interior, *J. Geophys. Res.*, *57*, 227–286, doi:10.1029/JZ057i002p00227.

Canup, R. M., and E. Asphaug (2001), Origin of the Moon in a giant impact near the end of the Earth's formation, *Nature*, *412*, 708–712, doi:10.1038/35089010.

Distin, P. A., S. G. Whiteway, and C. R. Masson (1970), Solubility of oxygen in liquid iron from 1785° to 1960°C. A new technique for the study of slag-metal equilibria, *Can. Metall. Q.*, *10*, 13–18.

Dubrovinsky, L., N. Dubrovinskaia, A. Kuznetsov, and I. Kantor (2005), Chemistry at extreme conditions: Approaching the Earth's major interface, in *Advances in High-Pressure Technology for Geophysical Applications*, edited by J. Chen et al., pp. 289–314, Elsevier, Amsterdam.

Dziewonski, A. M., and D. L. Anderson (1981), Preliminary reference Earth model, *Phys. Earth Planet. Inter.*, *25*, 297–356, doi:10.1016/0031-9201(81)90046-7.

Eaton, D. W., and J.-M. Kendall (2006), Improving seismic resolution of outermost core structure by multichannel analysis and deconvolution of broadband SmKS phases, *Phys. Earth Planet. Inter.*, *155*, 104–119, doi:10.1016/j.pepi.2005.10.007.

Egerton, R. F. (1996), *Electron Energy-Loss Spectroscopy in the Electron Microscope*, 485 pp., Springer, Berlin.

Fei, Y. W., and H. K. Mao (1994), In situ determination of the NiAs phase of FeO at high pressure and temperature, *Science*, *266*(5191), 1678–1680, doi:10.1126/science.266.5191.1678.

Fischer, W. A., and J. F. Schumacher (1978), Die Sättigungslöslichkeit von Reineisen an Sauerstoff von Schmelzpunkt bis 2046°C, ermittelt mit dem Schwebeschmelzverfahren, *Arch. Eisenhüttenwes*, *49*, 431–435.

Frost, D. J. (2003), Fe^{2+}-Mg partitioning between garnet, magnesiowüstite, and $(Mg,Fe)_2SiO_4$ phases of the transition zone, *Am. Mineral.*, *88*, 387–397.

Frost, D. J., U. Mann, Y. Asahara, and D. C. Rubie (2008), The redox state of the mantle during and just after core formation, *Philos. Trans. R. Soc., Ser. A*, *366*, 4315–4337, doi:10.1098/rsta.2008.0147.

Gessmann, C., and D. C. Rubie (1998), The effect of temperature on the partitioning of nickel, cobalt, manganese, chromium, and vanadium at 9 GPa and constraints on formation of the Earth's core, *Geochim. Cosmochim. Acta*, *62*, 867–882, doi:10.1016/S0016-7037(98)00023-4.

Haas, J. L., and B. S. Hemingway (1992), Recommended standard electrochemical potentials and fugacities of oxygen for the solid buffers and thermodynamic data in the systems iron-silicon-oxygen, nickel-oxygen, and copper-oxygen, *U.S. Geol. Surv. Open File Rep., 92-267*, 733 pp.

Halliday, A. N. (2007), Isotopic lunacy, *Nature*, *450*, 356–357, doi:10.1038/450356a.

Holzapfel, C., D. C. Rubie, D. J. Frost, and F. Langenhorst (2005), Fe-Mg interdiffusion in $(Mg,Fe)SiO_3$ perovskite and lower mantle reequilibration, *Science*, *309*, 1707–1710, doi:10.1126/science.1111895.

Kato, T., and A. E. Ringwood (1989), Melting relations in the system Fe-FeO at high pressure: Implications for the composition and formation of the Earth's core, *Phys. Chem. Miner.*, *16*, 524–538, doi:10.1007/BF00202207.

Kesson, S. E., J. D. Fitz Gerald, and J. M. Shelly (1998), Mineralogy and dynamics of a pyrolite lower mantle, *Nature*, *393*, 252–255, doi:10.1038/30466.

Knittle, E., and R. Jeanloz (1991), The high-pressure phase diagram of $Fe_{0.94}O$: A possible constituent of the Earth's core, *J. Geophys. Res.*, *96*, 16,169–16,180, doi:10.1029/90JB00653.

Kowalski, M., and P. J. Spencer (1995), Thermodynamic reevaluation of the Cr-O, Fe-O and Ni-O systems: Remodelling of the liquid, BCC and FCC phases, *Calphad*, *19*, 229–243, doi:10.1016/0364-5916(95)00024-9.

Lindsley, D. H. (1966), Pressure-temperature relations in the system FeO-SiO_2, *Year Book Carnegie Inst. Washington*, *65*, 226–230.

Mao, H. K., P. M. Bell, D. Shaner, and D. Steinberg (1978), Specific volume measurements of Cu, Mo, Pd, and Ag and calibration of the ruby R1 florescence pressure gauge from 0.06 to 1 Mbar, *J. Appl. Phys.*, *49*, 3276–3283, doi:10.1063/1.325277.

McCammon, C. (1993), Effect of pressure on the composition of the lower mantle end member Fe_xO, *Science*, *259*, 66–68, doi:10.1126/science.259.5091.66.

Miyajima, N., C. Holzapfel, Y. Asahara, L. S. Dubrovinsky, D. J. Frost, D. C. Rubie, M. Drechsler, K. Niwa, M. Ichihara, and T. Yagi (2010), Combining FIB milling and conventional argon ion milling techniques to prepare high quality site-specific TEM samples for quantitative EELS analysis of oxygen in molten iron, *J. Microsc.*, doi:10.1111/j.1365-2818.2009.03341.x, in press.

Murakami, M., K. Hirose, N. Sata, and Y. Ohishi (2005), Post-perovskite phase transition and mineral chemistry in the pyrolitic lowermost mantle, *Geophys. Res. Lett.*, *32*, L03304, doi:10.1029/2004GL021956.

O'Neill, H. S. C., D. Canil, and D. C. Rubie (1998), Oxide-metal equilibria to 2500°C and 25 GPa: Implications for core formation and the light component in the Earth's core, *J. Geophys. Res.*, *103*, 12,239–12,260, doi:10.1029/97JB02601.

O'Neill, H. S. C., M. I. Pownceby, and C. A. McCammon (2003), The magnesiowüstite-iron equilibrium and its implications for the activity-composition relations of $(Mg,Fe)_2SiO_4$ olivine solid solutions, *Contrib. Mineral. Petrol.*, *146*, 308–325, doi:10.1007/s00410-003-0496-4.

Ohtani, E., and A. E. Ringwood (1984), Composition of core, I. Solubility of oxygen in molten iron at high temperatures, *Earth Planet. Sci. Lett.*, *71*, 85–93, doi:10.1016/0012-821X(84)90054-2.

Ohtani, E., A. E. Ringwood, and W. Hibberson (1984), Composition of core, II. Effect of high pressure on solubility of FeO in molten iron, *Earth Planet. Sci. Lett.*, *71*, 94–103, doi:10.1016/0012-821X(84)90055-4.

Ozawa, H., K. Hirose, M. Mitome, Y. Bando, N. Sata, and Y. Ohishi (2008), Chemical equilibrium between ferropericlase and molten iron to 134 GPa and implications for iron content at the bottom of the mantle, *Geophys. Res. Lett.*, *35*, L05308, doi:10.1029/2007GL032648.

Ringwood, A. E. (1977), Composition of the core and implications for the origin of the Earth, *Geochem. J.*, *11*, 111–135.

Rubie, D. C., C. K. Gessman, and D. J. Frost (2004), Partitioning of oxygen during core formation on the Earth and Mars, *Nature*, *429*, 58–62, doi:10.1038/nature02473.

Rubie, D. C., F. Nimmo, and H. J. Melosh (2007), Formation of Earth's core, in *Treatise on Geophysics*, vol. 9, *Evolution of the Earth*, edited by D. J. Stevenson, pp. 51–90, Elsevier, Amsterdam.

Sakai, T., T. Kondo, E. Ohtani, H. Terasaki, N. Endo, T. Kuba, T. Suzuki, and T. Kikegawa (2006), Interaction between iron and post-perovskite at core-mantle boundary and core signature in plume source region, *Geophys. Res. Lett.*, *33*, L15317, doi:10.1029/2006GL026868.

Seagle, C. T., D. L. Heinz, A. J. Campbell, V. B. Prakapenka, and S. T. Wanless (2008), Melting and thermal expansion in the Fe-FeO system at high pressure, *Earth Planet. Sci. Lett.*, *265*, 655–665, doi:10.1016/j.epsl.2007.11.004.

Shen, G., P. Lazor, and S. K. Saxena (1993), Melting of wüstite and iron up to pressures of 600 kbar, *Phys. Chem. Miner.*, *20*, 91–96, doi:10.1007/BF00207201.

Takafuji, N., K. Hirose, M. Mitome, and Y. Bando (2005), Solubilities of O and Si in liquid iron in equilibrium with $(Mg, Fe)SiO_3$ perovskite and the light elements in the core, *Geophys. Res. Lett.*, *32*, L06313, doi:10.1029/2005GL022773.

Takahashi, E., K. Nakayama, and Y. Okamoto (2004), Phase relation in the system Fe-FeO up to 25 GPa, *Sci. Technol.*, *14*, 27.

Tanaka, S. (2007), Possibility of a low P wave velocity layer in the outermost core from global SmKS waveforms, *Earth Planet. Sci. Lett.*, *259*, 486–499, doi:10.1016/j.epsl.2007.05.007.

Tsuno, K., E. Ohtani, and H. Terasaki (2007), Immiscible two-liquid regions in the Fe-O-S system at high pressure: Implications for planetary cores, *Phys. Earth Planet. Inter.*, *160*, 75–85, doi:10.1016/j.pepi.2006.09.004.

van Cappellen, E. (1990), The parameterless correction method in X-ray microanalysis, *Microsc. Microanal. Microstruct.*, *1*, 1–22, doi:10.1051/mmm:01990001010100.

van Cappellen, E., and J. C. Doukhan (1994), Quantitative transmission X-ray microanalysis of ionic compounds, *Ultramicroscopy*, *53*, 343–349, doi:10.1016/0304-3991(94)90047-7.

Wiechert, U., A. N. Halliday, D. C. Lee, G. A. Snyder, L. A. Taylor, and D. Rumble (2001), Oxygen isotopes and the moon-forming giant impact, *Science*, *294*, 345–348, doi:10.1126/science.1063037.

Wood, B. J. (2000), Phase transformations and partitioning relations in peridotite under lower mantle conditions, *Earth Planet. Sci. Lett.*, *174*, 341–354, doi:10.1016/S0012-821X(99)00273-3.

Yakel, H. L. (1985), Crystal structures of stable and metastable iron-containing carbides, *Int. Metals Rev.*, *30*, 17–40.

Y. Asahara, High Pressure Material Physics Group, Department of Earth and Space Science, Graduate School of Science, Osaka University, 1-1 Machikaneyama-cho, Toyonaka 560-0043, Japan. (asaharay@anvil.ess.sci.osaka-u.ac.jp)

L. S. Dubrovinsky, D. J. Frost, N. Miyajima, and D. C. Rubie, Bayerisches Geoinstitut, Universität Bayreuth, D-95440 Bayreuth, Germany. (dan.frost@uni-bayreuth.de; dave.rubie@uni-bayreuth.de)

C. Holzapfel, Schleifring und Apparatebau GmbH, Am Hardtanger 10, D-82256 Fürstenfeldbruck, Germany. (c.holzapfel1@gmx.net)

E. Ohtani, M. Miyahara, and T. Sakai, Institute of Mineralogy, Petrology and Economic Geology, Tohoku University, Sendai 980-8578, Japan. (ohtani@mail.tains.tohoku.ac.jp; miyahara@ganko.tohoku.ac.jp; sakai@ganko.tohoku.ac.jp)